

# The XMM-Newton/2dF survey III: Comparison between optical and X-ray cluster detection methods

S. Basilakos<sup>1</sup>, M. Plionis<sup>1,2</sup>, A. Georgakakis<sup>1</sup>, I. Georgantopoulos<sup>1</sup>, T. Gaga<sup>1,3</sup>, V. Kolokotronis<sup>1</sup>, G. C. Stewart<sup>4</sup>

<sup>1</sup> *Institute of Astronomy & Astrophysics, National Observatory of Athens, I.Metaxa & B.Pavlou, Palaia Penteli, 152 36, Athens, Greece*

<sup>2</sup> *Instituto Nacional de Astrofísica, Óptica y Electrónica (INAOE) Apartado Postal 51 y 216, 72000, Puebla, Pue., Mexico*

<sup>3</sup> *Physics Department, Univ. of Athens, Panepistimioupolis, Zografou, Athens, Greece*

<sup>4</sup> *Department of Physics and Astronomy, University of Leicester, UK, LE1 7RH*

15 November 2018

## ABSTRACT

We directly compare X-ray and optical techniques of cluster detection by combining SDSS photometric data with a wide-field ( $\sim 1.6$  deg<sup>2</sup>) XMM-Newton survey near the North Galactic Pole region. The optical cluster detection procedure is based on merging two independent selection methods - a smoothing+percolation technique, and a Matched Filter Algorithm. The X-ray cluster detection is based on a wavelet-based algorithm, incorporated in the SAS v.5.3 package. The final optical sample counts nine candidate clusters with estimated APM-like richness of more than 20 galaxies, while the X-ray based cluster candidates are four. Three out of these four X-ray cluster candidates are also optically detected. We argue that the cause is that the majority of the optically detected clusters are relatively poor X-ray emitters, with X-ray fluxes fainter than the flux limit (for extended sources) of our survey  $f_x(0.3 - 2\text{keV}) \simeq 2 \times 10^{-14} \text{erg cm}^{-2} \text{s}^{-1}$ .

**Keywords:** galaxies: clusters: general - cosmology:observations - cosmology: large-scale structure of Universe.

## 1 INTRODUCTION

Clusters of galaxies occupy an eminent position in the structure hierarchy, being the most massive virialized systems known and therefore they appear to be ideal tools for testing theories of structure formation and extracting cosmological informations (cf. Bahcall 1988; West Jones & Forman 1995; Böhringer 1995; Carlberg et al. 1996; Borgani & Guzzo 2001; Nichol 2002 and references therein).

To investigate the global properties of the cosmological background it is necessary to construct and study large samples of clusters (cf. Borgani & Guzzo 2001). This understanding has initiated a number of studies aiming to compile unbiased cluster samples to high redshifts, utilizing multiwavelength data (e.g. optical, X-ray, radio). On the other hand, the study of individual clusters, provide complementary information regarding their physical properties and evolutionary processes. Overall, it is very important to fully understand the selection effects that enter in the construction of cluster samples since these could bias any statistical analysis of these samples (cf. Sutherland 1988).

At optical wavelengths there are several available samples in the literature. For example, the Abell/ACO

catalogue (Abell, Corwin & Olowin 1989) was constructed by visual inspection of the Palomar Observatory Sky Survey plates and is still playing an important role in astronomical research. Since then, a large number of optically selected samples constructed with automated methods have been constructed: EDCC (*Edinburgh Durham Cluster Catalogue*; Lumsden et al. 1992), APM (*Automatic Plate Measuring*; Dalton et al. 1994), PSCS (*Palomar Distant Cluster Survey*; Postman et al. 1996), EIS (*ESO Imaging Cluster Survey*; Olsen et al. 1999), RCS (*Red-Sequence Cluster Survey*; Gladders & Yee 2000) and the Sloan Digital Sky cluster survey (Goto et al. 2002; Bahcall et al. 2003). The above cluster samples, based on different selection methods, aim to obtain homogeneously selected optical cluster samples with redshifts that extended beyond the  $z \sim 0.2$  limit of the Abell/ACO catalogue. We should mention that the advantage of using optical data is the sheer size of the available cluster catalogues and thus the statistical significance of the emanating results.

A major problem here is that the optical surveys suffer from severe systematic biases which are due to projection effects. Background and foreground galaxies, projected on the cluster could distort the identifications (e.g. Frenk et al. 1990), which is particularly true for

poor systems at high redshifts. X-ray surveys provide an alternative method for compiling cluster samples, owing to the fact that the diffuse Intra-Cluster Medium (ICM) emits strongly at X-ray wavelengths. This emission is proportional to the square of the hot gas density, resulting in a high contrast with respect to the unresolved X-ray background, and thus X-ray selected clusters are less susceptible to projection effects. Therefore the main advantage, inherent in the X-ray selection of flux-limited samples is that the survey volume and hence number densities, luminosity and mass functions can be reliably computed. Furthermore, X-ray cluster surveys can be used to study cluster dynamics and morphologies, the Sunyaev Zeldovich effect and finally their cosmological evolution.

The first such sample, with large impact to the studies of clusters, was based on the Extended Einstein Medium Sensitivity Survey, containing 99 clusters (Stocke et al. 1991). The *ROSAT* satellite with its large field of view (FOV) and better sensitivity, allowed a leap forward in the X-ray cluster astronomy, producing large samples of both nearby and distant clusters (e.g. Castander et al. 1995; Ebeling et al. 1996a, 1996b; Scharf et al. 1997; Ebeling et al. 2000; Böhringer et al. 2001; Gioia et al. 2001; Böhringer et al. 2002; Rosati, Borgani & Norman 2002 and references therein). Recently, the *XMM-Newton* observatory with  $\sim 10$  times more effective area and  $\sim 5$  times better spatial resolution than the *ROSAT* provides an ideal platform for the study of galaxy clusters.

However, even with the improved sensitivity of the *XMM-Newton*, optical surveys still remain significantly more efficient and less expensive in telescope time for compiling cluster samples, albeit with the previously discussed limitations (eg. incompleteness, projection effects etc). Therefore it is necessary to study the different selection effects and biases that enter in detecting clusters in the two wavelength regimes. Donahue et al. (2002) using the *ROSAT* Optical X-ray Survey (ROXS), found that using both X-ray and optical methods to identify clusters of galaxies, the overlap was poor. About 20% of the optically detected clusters were found in X-rays while 60% of the X-ray clusters were identified also in the optical sample. Furthermore, not all of their X-ray detected clusters had a prominent red-sequence, a fact that could introduce a bias in constructing cluster samples using only colour information (as in Goto et al. 2002).

The aim of this work is along the same lines, attempting to make a detailed comparison of optical and X-ray cluster identification methods in order to quantify the selection biases introduced by these different techniques. We use *XMM-Newton* which has a factor of  $\sim 5$  better spatial resolution and an order of magnitude more effective area at 1 keV, making it an ideal instrument for the detection of relatively distant clusters.

The plan of the paper is as follows. The observed data sets are presented in Section 2. In Section 3 we discuss the methods employed to identify candidate optical clusters and comment on the systematic effects introduced in our analysis. Also, Section 3 describes our projected cluster shape determination method as well

as the cluster surface brightness based on a King like profiles. In Section 4 we compare the optical and X-ray selected cluster samples. Finally, in Section 5, we present our conclusions. Throughout this paper we use  $H_0 = 100h$  km s $^{-1}$ Mpc $^{-1}$  and  $\Omega_m = 1 - \Omega_\Lambda = 0.3$ .

## 2 OBSERVATIONS

### 2.1 The optical data

In our analysis we use the SDSS Early Data Release (EDR), covering an area of  $\sim 400\text{deg}^2$  in the sky (Stoughton et al. 2002). The SDSS is an ongoing imaging and spectroscopic survey that covers  $\sim 10000$  deg $^2$  of the sky. Photometry is obtained in five bands ( $u, g, r, i, z$ ) to the limiting magnitude  $r \lesssim 22.5$  mag, providing an homogeneous multi-color photometric catalogue.

Goto et al. (2002), applied an object cluster finding algorithm to the SDSS EDR and produced a list of galaxy clusters (hereafter CE catalogue), with estimated photometric redshifts which contains 2770 and 1868 galaxy clusters in the North and South slices, respectively. The cluster redshifts were estimated using color information by identifying the bin in  $g - r$  which has the largest number of galaxies around the color prediction of elliptical galaxies (Fukugita, Shimasaku, Ichikawa 1995) at different redshifts (which define the different  $g - r$  bins). Note that the true and estimated redshifts are better correlated for  $z < 0.3$ , with rms scatter  $\sim 0.015$ , while for  $z > 0.3$  it is  $\sim 0.021$ . Note, that the CE method is optimized up to  $z \leq 0.4$  and becomes highly insensitive at higher redshifts.

### 2.2 The XMM-Newton data

We analyzed 9 *XMM-Newton* fields with nominal exposure times between 2 and 10 ksec. The *XMM-Newton* field-of-view is a circle with a radius of 15 arcmin and thus our survey covers an area of 1.8 deg $^2$ . However, one of the fields, suffering from significantly elevated and flaring particle background, was excluded from the X-ray analysis. This reduces our effective area to 1.6 deg $^2$ . The details of the X-ray observations are given in Georgakakis et al. (2004) and Georgantopoulos et al. *in preparation*.

## 3 OPTICAL CLUSTER DETECTION

Identifying real clusters using imaging data is a difficult task since projection effects can significantly affect the visual appearance of clusters. Many different algorithms have been proposed and applied on different data sets. In what follows we present a new cluster finding algorithm (based on two distinct algorithms) and apply it on the subsample of the  $r$ -band SDSS data $^*$ , that overlaps with our *XMM-Newton* survey.

\* We have tested that our results remain qualitatively unaltered when using the  $i$ -band.

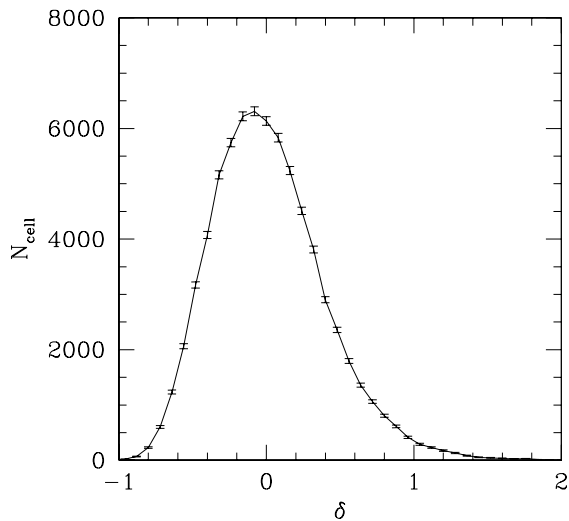


**Figure 1.** The SDSS probability density function (*pdf*).

### 3.1 The Smoothing+Percolation Procedure

This cluster detection algorithm (hereafter SMP method) is based on smoothing the discrete distribution using a Gaussian smoothing kernel on a  $N_{gr} \times N_{gr}$  grid:

$$\mathcal{W}(|\mathbf{x}_i - \mathbf{x}_{gr}|) = \frac{1}{\sqrt{2\pi R_{sm}^2}} \exp\left(-\frac{|\mathbf{x}_i - \mathbf{x}_{gr}|^2}{2R_{sm}^2}\right), \quad (1)$$

with  $R_{sm}$  the smoothing radius in grid-cell units and  $\mathbf{x}_i$  the Cartesian position of the  $i^{th}$  galaxy. The smoothed surface density, of the  $j^{th}$  cell at the grid-cell positions  $\mathbf{x}_{gr}$ , is:

$$\rho_j(\mathbf{x}_{gr}) = \frac{\sum_i \rho_j(\mathbf{x}_i) \mathcal{W}(|\mathbf{x}_i - \mathbf{x}_{gr}|)}{\int \mathcal{W}(|\mathbf{x}_i - \mathbf{x}_{gr}|) d^2x}, \quad (2)$$

where the sum is over the distribution of galaxies with positions  $\mathbf{x}_i$ . For each cell we define its density fluctuation,  $\delta_j$ , as:

$$\delta_j = \frac{\rho_j(x_{gr}) - \langle \rho \rangle}{\langle \rho \rangle}, \quad (3)$$

where  $\langle \rho \rangle$  is the mean projected SDSS galaxy density and the probability density function,  $f(\delta)$ , which is plotted in Fig. 1. We select all grid-cells with overdensities above a chosen critical threshold ( $\delta \geq \delta_{cr}$ ) and then we use a friends-of-friends algorithm to link all adjacent cells in order to form groups of connected cells, which we consider as our candidate clusters. Note that the grid cell size is such that at  $z = 0.4$  it corresponds to  $100 h^{-1} \text{kpc}$  ( $\sim 19''$ ).

There are three free parameters in the above procedure: the critical overdensity threshold ( $\delta_{cr}$ ) the smoothing radius ( $R_{sm}$ ) and the number of connected cells ( $n_c$ ) above which we consider a candidate cluster. Due to the fact that clusters should be identified as high density regions, we choose the critical value of the overdensity to be  $\delta_{cr} \simeq 1$  which corresponds to the  $\sim 98$  percentile of

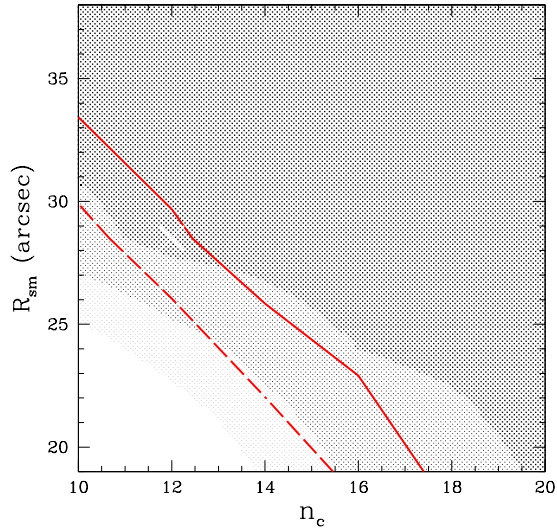


**Figure 2.** Statistical significance of our cluster detection procedure as a function of the smoothing radius  $R_{sm}$  and minimum number of connected cells,  $n_c$ . The darkest greyscale corresponds to  $\mathcal{P} = 0.96$ , while the faintest to  $\mathcal{P} < 0.88$ . The continuous line corresponds to the expected number of APM clusters, while the broken line to the number Goto et al. (2002) clusters. The cross reflects our best choice of the free parameters ( $R_{sm}$  and  $n_c$ ).

the probability density function (*pdf*) plotted in Fig.1. Had we used lower values of  $\delta_{cr}$  we would have percolated overdense regions through large parts of the whole area.

The  $R_{sm}$  and  $n_c$  parameters were chosen in such a way as to minimize the number of spuriously detected clusters. To this end we perform a series of Monte-Carlo simulations in which we randomize the positions of the SDSS galaxies, destroying its intrinsic clustering, while keeping unchanged the galaxy redshift selection function. On this intrinsically random galaxy distribution we apply the procedure described above, by varying the values of the free parameters ( $R_{sm}$  and  $n_c$ ). We define the probability of detecting real clusters in the SDSS data, as  $\mathcal{P}(R_{sm}, n_c) = 1 - N_{rand}/N_{SDSS}$ , were  $N_{rand}$  is the number of clusters detected in the randomized distribution and  $N_{SDSS}$  is the number of clusters detected in the true SDSS data. In Fig. 2 we show as a greyscale these probabilities. Although, increasing  $R_{sm}$  and  $n_c$ , results in very high probabilities of detecting real high-density regions, it also results in small numbers of detected clusters. We therefore attempt to break this degeneracy by using the expected number of clusters from existing surveys. For example, the continuous line in Fig.2 corresponds to the expected number of APM clusters in the area covered by our XMM/2dF survey<sup>†</sup>, while the thick

<sup>†</sup> This number ( $\sim 40$ ) is estimated, without assuming any evolution, by multiplying the local ( $z < 0.1$ ) mean number density of APM clusters with the volume element covered by our survey out to a  $z \sim 0.45$  within the concordance cosmological model ( $\Omega_\Lambda = 0.7$ ).

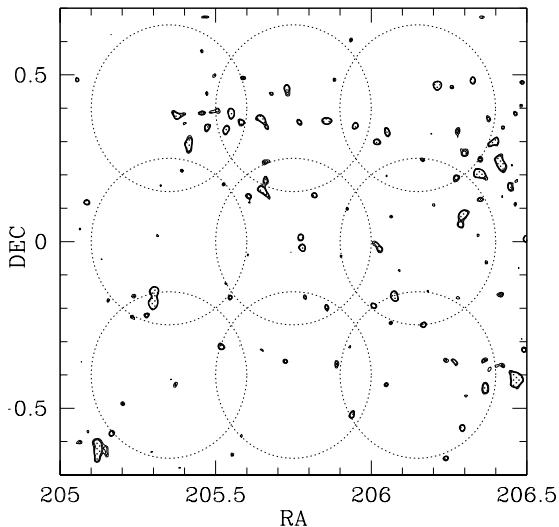


**Figure 3.** The smooth SDSS density field on equatorial coordinates. The  $\delta_{\text{cr}} = 1$  level appears as a thick continuous line. The large dotted circles represent the XMM 15 arcmin radius fields of view of our shallow XMM/2dF survey.

broken line delineates the corresponding number of the Goto et al. (2002) clusters. The region of the highest probability, that falls within the above cluster number limits, is that corresponding to:

$$R_{\text{sm}} = 28.5'' \quad n_c = 12 ,$$

which we choose as our optimal parameters for the detection of real clusters.

In Fig. 3 we plot the smoothed SDSS galaxy distribution, using the above value of  $R_{\text{sm}}$ , on the equatorial plane with a contour step of  $\Delta\delta = 0.2$ , starting from  $\delta_{\text{cr}} = 1$ . Many overdense regions are apparent. Finally, we note that our cluster finding algorithm with  $n_c = 12$  produces a total of 25 candidate clusters, 11 of which are common with the Goto et al. (2002) sample of 29 clusters in the same region.

### 3.2 The Matched Filter Algorithm

In addition to the SMP technique we have also employed the matched filter algorithm (hereafter MFA) described by Postman et al. (1996) to identify optical galaxy overdensities. The advantage of this method is that it exploits both positional and photometric information producing galaxy density maps where spurious galaxy fluctuations are suppressed. Also, an attractive feature of this method is that it provides redshift estimates for the detected candidate galaxy clusters. A drawback of the matched filter method is that one must assume a form for the cluster luminosity function and radial profile. Clusters with the same richness but different intrinsic shape or different luminosity function from the assumed ones do not have the same likelihood of being detected.

A detailed description of the matched filter algorithm can be found in Postman et al. (1996). In brief, the

filter used to convolve the galaxy catalogue is derived from an approximate maximum likelihood estimator obtained from a model of the spatial and luminosity distribution of galaxies within a cluster. At any given patch of the sky the number density of galaxies per magnitude bin is

$$D(r, m) = b(m) + \Lambda_{cl} P(r/r_c) \phi(m - m^*) , \quad (4)$$

where  $D(r, m)$  is the galaxy surface density (cluster+field galaxies) at a given magnitude  $m$  and at a distance  $r$  from the galaxy cluster center,  $b(m)$  is the field galaxy surface density,  $P(r/r_c)$  is the cluster projected radial profile,  $\phi(m - m^*)$  is the cluster luminosity function and  $\Lambda_{cl}$  is an estimator of the cluster richness. The parameters  $r_c$  and  $m^*$  are the characteristic cluster scale length and apparent magnitude corresponding to the characteristic luminosity of the cluster luminosity function. Postman et al. (1996) showed that the filter for cluster detection should maximize the expression

$$\int P(r/r_c) \frac{\phi(m - m^*)}{b(m)} D(m, r) d^2r dm . \quad (5)$$

Assuming that the galaxy distribution  $D(m, r)$  can be represented by a series of  $\delta$ -functions at the observed positions and magnitudes, the integral above is reduced to

$$S(i, j) = \sum_{k=1}^{N_T} P(r_k/r_c) L(m_k) , \quad (6)$$

where  $L(m_k)$  is defined as

$$L(m) = \frac{\phi(m - m^*)}{b(m)} . \quad (7)$$

The quantity  $S(i, j)$  is the value of the  $(i, j)$  pixel of the convolved galaxy density map and  $N_T$  is total number of galaxies in the catalogue.  $L(m_k)$  is the luminosity weighting function (i.e. flux filter). In practice, the survey area is binned into pixels  $(i, j)$  of given size (for the choice of values see below) and the sum in equation 6 is evaluated by iterating through all galaxies in the catalogue. This then is repeated for every pixel of the density map. Both  $m^*$  and  $r_c$  are a function of redshift and hence  $S(i, j)$  also depends on redshift through these parameters. The redshift dependence of  $m^*$  also includes a  $k$ -correction as discussed in the next section.

The flux filter in equation 7 has a divergent integral at faint magnitudes for Schechter luminosity functions with  $\alpha < -1$ . To overcome this problem Postman et al. (1996) modified the flux filter by introducing a power-law cutoff of the form  $10^{-0.4(m - m^*)}$ . Therefore, the flux filter in equation 6 is defined as:

$$L(m) = \frac{\phi(m - m^*) 10^{-0.4(m - m^*)}}{b(m)} . \quad (8)$$

The radial filter in equation 6 is defined:

$$P(r) = \frac{1}{\sqrt{1+(r/r_c)^2}} - \frac{1}{\sqrt{1+(r_{co}/r_c)^2}}, \quad \text{if } r < r_{co} \\ 0 \quad \text{otherwise,} \quad (9)$$

where  $r_c$  is the cluster core radius and  $r_{co}$  is an arbitrary cutoff radius. Here, we assume  $r_c = 100 h^{-1}$  kpc and  $r_{co} = 1 h^{-1}$  Mpc. The characteristic absolute magnitude

of the luminosity function, in  $r$ -band is taken to be  $M^* = -20.83 + 5\log h$  (Blanton et al. 2003). Both the radial and the flux filter are normalized as described in Postman et al. (1996).

### 3.2.1 The MFA Cluster detection

The matched filter algorithm is applied to a  $1.6 \text{ deg}^2$  subregion of the SDSS centered on our XMM/2dF survey. We consider galaxies with magnitudes brighter than  $r = 22.5 \text{ mag}$ . At fainter magnitudes the SDSS is affected by incompleteness. The galaxy density map  $S(i, j)$  representing the galaxy density map is independently estimated for redshifts between  $z_{\min} = 0.1$  to  $z_{\max} = 0.6$ , incremented in steps of 0.1. The  $z_{\max}$  corresponds to the redshift where  $m^*$  becomes comparable to the limiting magnitude of the survey. The characteristic luminosity,  $L^*$ , the faint end slope of the luminosity function,  $\alpha$ , and the cluster core radius,  $r_c$ , are assumed to remain constant with redshift.

The conversion from luminosity to apparent magnitude requires an assumption to be made on the  $k$ -correction of the galaxies. Here we assume a non-evolving elliptical galaxy model obtained from the Bruzual & Charlot (1993) stellar population synthesis code (Pozzetti, Bruzual & Zamorani 1996). It is important to (hereafter SMP method) emphasize that the choice of  $k$ -correction does not significantly affect the cluster detections, but has an impact on the redshift determination.

The pixel size of the galaxy density maps at any redshift is taken to be  $\approx 19''$  corresponding to a projected cluster core radius of  $r_c = 100 h^{-1} \text{ kpc}$  at the redshift  $z = 0.4$  (see section 3.1). Galaxy density maps are created for redshifts 0.1–0.6 and stored in FITS images. The peaks of the galaxy distribution are detected using SExtractor (Bertin & Arnouts 1996). The mean and the variance of the background are determined using a global value in each likelihood map. The main input parameters are the detection threshold,  $\sigma_{\text{det}}$ , given as a multiple of background variance, and the minimum number of pixels,  $N_{\min}$  for a peak to be extracted as candidate cluster. Simulations have been carried out (see next section) to optimize these parameters and to minimize the number of spurious cluster detections ( $\approx 5\%$ ). We adopt  $\sigma_{\text{det}} = 4.0$  while  $N_{\min}$  is set to the area of a circle with radius  $r_c = 100 h^{-1} \text{ kpc}$  at any given redshift.

The significance of a detection,  $\sigma$ , is defined as the maximum value of all the pixels associated with that detection (i.e. pixels with values above the SExtractor detection threshold), expressed in multiples of the rms noise above the background. The peaks (i.e. candidate clusters) extracted on density maps of different redshifts are matched by positional coincidence using a radius of  $\approx 1 \text{ arcmin}$ . The approximate redshift of the candidate cluster is taken to be the redshift where the detection significance is maximum.

Within the area of our XMM/2dF survey the MFA method identifies 12 cluster candidates out of which 6 are found also by Goto et al. (2002) and 9 are found by the SMP method.

### 3.2.2 The MFA simulations

Monte Carlo simulations similar to those described in section 3.2 were employed to test the performance of the matched filter algorithm and to establish the best choice of extraction parameters. A total of 100 random galaxy catalogues over an area of  $\sim 1.6 \text{ deg}^2$  (i.e. similar to that covered by the real catalogue) were produced with the same magnitude distribution as the real dataset. The matched filter algorithm was then applied to these mock catalogues and the SExtractor was used to identify peaks in the derived density maps.

Following Olsen et al. (1999) we minimize the number of spurious detections using the SExtractor parameters  $N_{\min}$  and  $\sigma_{\text{det}}$  as well as other properties of the noise peaks such as the number of redshifts where a peak is detected,  $n_z$ . We adopt  $\sigma_{\text{det}} = 4$ ,  $N_{\min} = \pi r_c^2$  at any given redshift and we only consider peaks that appear in at least two consecutive redshifts (i.e.  $n_z \geq 2$ ). For this choice of parameters we estimate the spurious cluster contamination to be  $\approx 5\%$ .

## 3.3 Our final optically selected cluster sample

We construct our final optical cluster catalogue by adopting the conservative approach of considering as cluster candidates those identified by both the SMP and MFA techniques. Our final sample, which we call SMPMFA, consists of 9 clusters with SDSS richness of more than 20 galaxies, corresponding roughly to APM type clusters. This estimated richness corresponds to the number of galaxies having  $r$ -band magnitudes  $\leq m_3 + 2$  (where  $m_3$  is the magnitude of the third brightest cluster member) within a radius of  $0.75 h^{-1} \text{ Mpc}$ , estimated using the approximate redshift of the cluster.

Comparing our SMPMFA sample with the 29 clusters of Goto et al. (2002), we find 5 in common.

### 3.3.1 Cluster Shapes

We investigate the reality of our candidate clusters by fitting a King's profile to their projected galaxy distribution. We expect that a galaxy enhancement produced by projection effects should have a rather flat profile and thus the goodness of fit should be low<sup>‡</sup>. The King's profile is given by:

$$\Sigma(\theta) \propto \left[ 1 + \left( \frac{\theta}{\theta_c} \right)^2 \right]^{-\alpha}, \quad (10)$$

where  $\theta_c$  is the angular cluster core radius. The slope  $\alpha$  is related to  $\beta$ , the ratio of the specific energy in galaxies to the specific thermal energy in the gas, by  $\alpha = (3\beta - 1)/2$  and spans the range  $0.6 \lesssim \alpha \lesssim 1$  (cf. Bahcall & Lubin 1993; Girardi et al. 1995; Girardi et al. 1998).

In order to quantify the parameters of the fit we perform a standard  $\chi^2$  minimization procedure between

<sup>‡</sup> Note however that a real cluster with significant substructures could also produce a rather poor King's profile

**Table 1.** List of the SDSS clusters in the XMM area. The correspondence of the columns is as follows: index number, right ascension  $\alpha$  and declination  $\delta$  of the cluster center, cluster ellipticity  $\epsilon$  and  $\phi$  is the cluster position angle (in degrees), the cross correlation results (C-C)- the numbers correspond to: 1 - CE method, Goto et al. (2002); 2 - Matched Filter Algorithm; 3 - X-ray extended sources (Gaga et al. *in preparation*); 4 - Couch et al. (1991). The next columns are: the estimated redshift by different methods, the core radius with its  $2\sigma$  error and the  $\chi^2$  probabilities ( $P_{\chi^2}$ ) of consistency between the intrinsic cluster density profile and King model. Finally,  $\mathcal{N}_g$ ,  $m_3$  and  $f_x$  are the number of galaxies, the magnitude of the third-brightest cluster member (within a radius  $\sim 0.75 h^{-1}$  Mpc) and the detected flux or the  $3\sigma$  upper flux limits in units of  $10^{-14}$  erg  $\text{cm}^{-2} \text{s}^{-1}$  respectively (for details see section 4). Note that the  $r_c$  has units of  $h^{-1}$  Mpc and the King profile slope used  $\alpha \simeq 0.7$ .

Index	$\alpha$	$\delta$	$\epsilon$	$\phi$	C-C	$z$	$r_c$	$P_{\chi^2}$	$\mathcal{N}_g$	$m_3$	$f_x$
1	205.513	-0.316	0.10	113.7	2	0.10 <sup>2</sup>	0.10 $\pm$ 0.03	0.14	29	17.38	<0.40
2	205.417	0.287	0.56	6.3	1,2,3	0.39 <sup>1</sup> - 0.40 <sup>2</sup>	0.50 $\pm$ 0.17	0.003	26	18.96	1.86
3	205.307	-0.183	0.61	4.7	1,2	0.40 <sup>1</sup> - 0.60 <sup>2</sup>	0.39 $\pm$ 0.13	0.73	34	19.37	<0.16
4	205.550	0.378	0.37	170.4	1,2	0.31 <sup>1</sup> - 0.50 <sup>2</sup>	0.52 $\pm$ 0.17	0.95	49	19.76	<3.91
5	205.859	0.354	0.37	90.7	2	0.60 <sup>2</sup>	0.56 $\pm$ 0.19	0.50	50	20.06	<6.37
6	205.777	-0.022	0.10	158.2	2,3,4	0.60 <sup>2</sup> - 0.67 <sup>4</sup>	0.35 $\pm$ 0.11	0.98	33	20.03	5.55
7	206.296	0.078	0.56	22.0	1,2	0.37 <sup>1</sup> - 0.30 <sup>2</sup>	0.42 $\pm$ 0.14	0.59	30	19.25	<7.29
8	206.363	-0.438	0.43	3.3	2	0.30 <sup>2</sup>	0.46 $\pm$ 0.15	0.63	29	19.49	<3.29
9	206.210	0.468	0.10	48.0	1,2,3	0.36 <sup>1</sup> - 0.30 <sup>2</sup>	0.09 $\pm$ 0.03	0.46	28	19.56	6.03

the measured surface density of each of our clusters and eq.(10):

$$\chi^2 = \sum_{i=1}^n \left[ \frac{\Sigma_{\text{data}}^i(\theta) - \Sigma_{\text{King}}^i(\theta, \theta_c, \alpha)}{\sigma^i} \right]^2. \quad (11)$$

In Table 1 we present our cluster positions and the parameters of the King's profile, as well as the  $\chi^2$  probability ( $P_{\chi^2}$ ) of consistency between the King's profile and the cluster density profile. The errors are  $2\sigma$  estimates, corresponding to  $\Delta\chi^2 = 6.17$  ( $\Delta\chi^2 \equiv \chi^2 - \chi_{\text{min}}^2$ , with  $\chi_{\text{min}}^2$  the absolute minimum value of the  $\chi^2$ ). All but one candidate clusters are well fitted by a King's profile with  $P_{\chi^2} \geq 0.14$ , while the slope  $\alpha$  of the profile is  $\simeq 0.7$ , corresponding to a  $\beta$ -parameter of  $\simeq 0.8$  (cf. Cavaliere & Fusco-Femiano 1976; Jones & Forman 1999). Furthermore, we present the estimated cluster redshifts (either from Goto et al. 2000 or from the MFA method). In the case of cluster # 6 we give the spectroscopic redshift from Couch et al. (1991).

For those clusters which are well fitted by a King-like profile we can give an approximation regarding their spatial core radius ( $r_c$ ). Different studies (Girardi et al. 1995; Girardi et al. 1998), have shown that the radial core radius of Abell clusters has an average value of  $\bar{r}_c \simeq 0.10 - 0.15 h^{-1}$  Mpc. Therefore, having an estimate of the cluster redshift, the corresponding core radius can be easily found from  $r_c = d_L \tan(\theta_c)$ , where  $d_L$  is the luminosity cluster distance.

In order to check for possible evolutionary trends regarding the cluster core, we have plotted the core radius as a function of redshift. As shown in Fig.4 we find a significant correlation; the coefficient is  $\sim 0.60$  with the probability of zero correlation being  $\leq 10^{-5}$ . In the local universe ( $0 \leq z \leq 0.15$ ), the core radius is approximately equal with  $\sim 0.10 h^{-1}$  Mpc, which is similar to the value derived by Girardi et al. (1998). The line of the best fit is given by

$$r_c \simeq 0.530(\pm 0.291)z + 0.138(\pm 0.134). \quad (12)$$

In order to check if the observed evolutionary trend is an artifact of possible systematic effects, we have

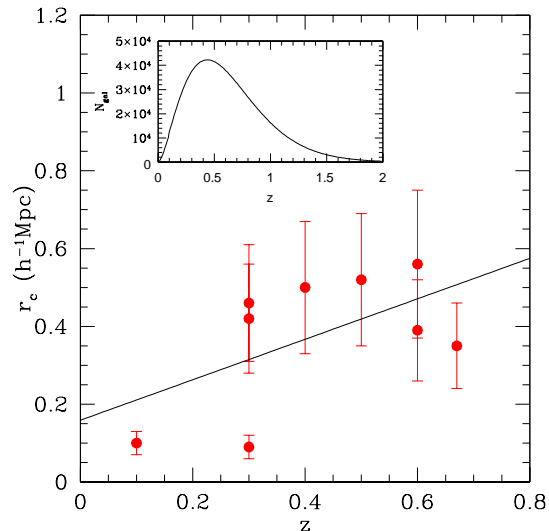


**Figure 4.** The cluster core radius ( $r_c$ ) redshift correlation for the analyzed SMPMFA. In the insert we show the SDSS redshift selection function using the Blanton et al. (2003) luminosity function.

firstly investigated the effect of the SDSS redshift selection function. We have determined the predicted SDSS redshift distribution using the  $r$ -band luminosity function of Blanton et al. (2003) for galaxies between  $0.02 \leq z \leq 0.22$ . We have extrapolated their luminosity dependent density evolution model up to  $z = 2$  and find that the SDSS redshift distribution increases up to  $z \sim 0.45$  (insert of Fig. 4). This implies that the sample is roughly volume limited out to this distance and thus the  $r_c - z$  trend seen in Fig.4 should not be due to systematic effects related to undersampling of the cluster galaxy population. Since we have used a single band ( $r$ -band) to detect clusters, we also explore the effect of determining their morphological characteristics in different rest-frame bands. We note that the wavelength difference (effective  $\lambda$ ) between the Sloan  $r$  and  $z$  bands

is  $\sim 2800 \text{ \AA}$ , which corresponds to a redshift difference of  $\sim 0.45$ . Therefore, the rest-frame r-band at low redshifts ( $z \lesssim 0.15$ ) roughly shifts to the z-band at  $z \sim 0.6$ . We then compare the mean core-radius of our most distant clusters (at  $\sim 0.6$  and  $0.67$ ) using the z-band (within its completeness limit  $m_z \leq 21.5$ ) with the mean core-radius of our relatively nearby clusters ( $z < 0.3$ ) determined in the r-band (within its the completeness limit of  $m_r \leq 22$ ). We find that the r-band core radius of the 4 low- $z$  clusters is  $0.27 \pm 0.19$  while the z-band core radius of the 2 high- $z$  clusters is  $0.65 \pm 0.35$ . Therefore it seems that the effect of the different rest-frame bands in the definition of the cluster morphology (at least for our sample and the redshifts covered) does neither create nor mask the observed evolutionary trend.

We list in Table 1 the cluster shape parameters determined by using the moments of inertia method (cf. Carter & Metcalfe 1980; Basilakos, Plionis, Maddox, 2001). This method is based in evaluating the moments  $I_{11} = \sum \delta_j (r_j^2 - x_j^2)$ ,  $I_{22} = \sum \delta_j (r_j^2 - y_j^2)$ ,  $I_{12} = I_{21} = -\sum \delta_j x_j y_j$ , where  $\delta_j$  is the galaxy overdensity of each cell and  $x, y$  are the Cartesian coordinates of each cell, after transforming the equatorial coordinates into an equal area coordinate system, centered on the cluster center. Then, diagonalizing the inertia tensor

$$\det(I_{ij} - \lambda^2 M_2) = 0 \quad (M_2 \text{ is } 2 \times 2 \text{ unit matrix.}) \quad (13)$$

we obtain the eigenvalues  $\lambda_1, \lambda_2$ , from which we define the ellipticity of the configurations under study by:  $\epsilon = 1 - \lambda_2/\lambda_1$ , with  $\lambda_1 > \lambda_2$ . The corresponding eigenvectors provide the direction of the principal axis. It is evident that 3 out of 9 clusters have large projected ellipticities ( $\epsilon > 0.5$ ).

## 4 COMPARING CLUSTERS IN THE OPTICAL & X-RAY BANDS

### 4.1 X-ray Cluster Detection

The full details of the cluster detection procedure and the cluster X-ray luminosity and temperature determinations will be described in Gaga et al. (*in preparation*). Here we only briefly present the main method and results.

In order to detect candidate clusters in our XMM fields we use the soft 0.3-2 keV data since this band maximizes the signal to noise ratio especially in the case of relatively low temperature galaxy clusters. In particular we use the *EWAVELET* detection algorithm of the *XMM-Newton* SAS v.5.3 analysis software package, which detects sources on the wavelet transformed images.

We search for sources down to the  $5\sigma$  detection threshold, on the PN and the co-added MOS1 and MOS2 detector images, separately. The output list is fed into the *SAS EMLDETECT* algorithm which performs a maximum likelihood PSF fit on each source yielding a likelihood for the extension. We are using an extension likelihood threshold corresponding to a level of less than  $\sim 0.5\%$  spurious extended sources. We have detected 7 candidate clusters on the MOS mosaic, while 5 extended

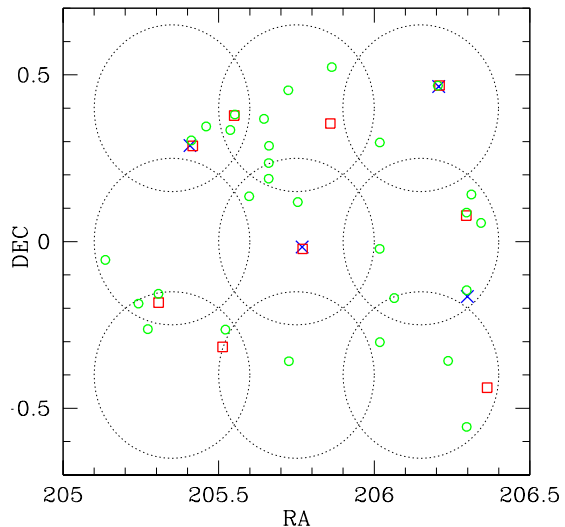


**Figure 5.** The candidate cluster positions within our shallow XMM-Newton survey. Open squares are the optically selected clusters using the SMPMFA technique while open circles are the Goto et al. (2002) clusters. Crosses are X-ray selected clusters of Gaga et al. (in preparation 2004). The large dotted circles represent the 15 arcmin radius XMM fields of view covered by our shallow XMM survey.

sources were detected on the PN images, out of which 3 overlap with the MOS candidates.

We have also visually inspected the candidate clusters and found that in some occasions the high extension likelihood was due to multiple point sources (confusion). These spurious detections are excluded from our final X-ray selected cluster candidate list. This results in a final list of 4 X-ray cluster candidates, out of which 2 are detected on both the MOS and PN, one is detected only on the MOS (there was no valid PN image) and the last one is detected only on the PN (note that this cluster was detected with a slightly smaller likelihood probability,  $\sim 0.99$ ). The faintest extended source has a flux of  $\sim 2 \times 10^{-14} \text{ erg cm}^{-2} \text{ s}^{-1}$ . Note that for the (0.3-2) keV energy band the net X-ray count rate for our detected extended sources is 3 to  $7 \times 10^{-3} \text{ cts s}^{-1}$ , within a  $30''$  radius circle.

In Table 2 we present the properties of the X-ray cluster candidates.

### 4.2 The optical versus X-ray cluster detections

We perform a cross-correlation between the different cluster catalogues (optical, X-rays), using a 3 arcmin matching radius to identify common objects. In Fig. 5, we plot the positions of (a) our optically detected cluster candidates (SMPMFA sample), (b) the Goto et al. (2002) clusters and (c) the X-ray detected XMM-Newton clusters. All four X-ray detections coincide with optical cluster candidates from different methods, with the largest coincidence rate (3 out of 9) being with our SMPMFA optical candidates. The most distant cluster in our SMPMFA sample, located at  $\alpha = 13^{\text{h}} 43^{\text{m}} 5^{\text{s}}$  sec

**Table 2.** The X-ray cluster properties: (1) and (2) equatorial coordinates (J2000) (2) X-ray Luminosity ( $\text{erg s}^{-1}$ ) in the 0.3-2 keV band, (3) X-ray flux (0.3-2) keV, in units of  $10^{-14} \text{erg sec}^{-1}, \text{cm}^{-2}$ , (4) cluster temperature from Gaga et al. (in preparation 2004), (5) the XMM field, (6) optical follow up and finally, the cluster redshift. Note that the subscripts 1,2 and 4 are the same as in Table 1.

$\alpha$	$\delta$	$L_x$	$f_x$	$T(\text{keV})$	XMM-Field	Optical	$z$	detector
13 41 39.1	+00 17 39.3	$10^{42.63}$	1.86	$\sim 3$	F864-1	SMPMFA+CE	$0.40^2$	PN+MOS
13 43 04.8	-00 00 56.3	$10^{43.60}$	5.55	$\sim 2$	F864-5	SMPMFA	$0.67^4$	PN+MOS
13 45 11.9	-00 09 52.6	$10^{42.00}$	5.05	$\sim 1$	F864-6	CE	$0.12^1$	MOS
13 44 49.7	+00 27 53.3	$10^{42.87}$	6.03	$\sim 1$	F864-3	SMPMFA+CE	$0.30^2$	PN

**Table 3.** Cross correlations results. The correspondence of the columns is as follows: comparison pair and the number of common clusters.

Methods compared	Number of common clusters
SMPMFA - CE	5
SMPMFA - X-rays	3
CE - X-rays	3

$\delta = 00^\circ 00' 56''$ , found also in X-rays, is missed by Goto et al. (2002).

The cross-correlation results between the different cluster detection methods are presented in Table 3, which in the first column lists the comparison method pair and in the second column the number of common objects.

It is interesting that our SMPMFA combined method finds 3 out of the 4 X-ray clusters, missing the nearest one, which from its X-ray luminosity appears to be a group of galaxies, rather than a cluster. However, there are still 6 SMPMFA clusters that do not appear to have X-ray counterparts, for which we give their  $3\sigma$  flux upper limits (see Table 1 last column). Conversion from count rate to flux was done assuming a bremsstrahlung spectrum with 3 keV. The flux was measured in a  $30''$  radius cell and the correction to the total flux was performed taking into account a King profile with  $r_c = 150 h^{-1} \text{kpc}$ . This could be a hint that these clusters are either the results of projection effects (which however cannot explain the good King profile fits - see Table 1), or that our XMM-Newton survey is too shallow to reveal the probably weak X-ray emission from these clusters.

In order to address this issue and to study the relation between the limiting flux of our X-ray survey with respect to exposure time, we have carried out the following experiment. We have analysed observations taken from 15 XMM-Newton public fields with mean exposure times  $\sim 21$  ksec in the soft 0.3-2 keV band, after filtering to correct for high particle background periods. Using the parameters of the SAS software as described previously, we have detected 31 candidate clusters. The faintest cluster detected, with a flux of  $\sim 5 \times 10^{-15} \text{erg cm}^{-2} \text{s}^{-1}$ , was found in the deepest field with an exposure time of 37 ksec. We then reduce the exposure times to a new mean value of  $\sim 5$  ksec, similar to our shallow survey, and find only 9 out of the 31 previously identified candidate clusters (29%), having a limiting flux of  $\sim 2.3 \times 10^{-14} \text{erg cm}^{-2} \text{s}^{-1}$ . Therefore, had we had

deeper XMM-Newton observations (by an average factor of  $\sim 5$  in exposure time) we would have detected  $\sim 13$  X-ray candidate clusters in the region covered by our shallow XMM-Newton/2dF survey, which is consistent (within  $1\sigma$ ) with the number of our SMPMFA cluster candidates.

## 5 CONCLUSIONS

We have made a direct comparison between optical and X-ray based techniques used to identify clusters. We have searched for extended emission in our shallow XMM-Newton Survey, which covers a  $\sim 1.6 \text{deg}^2$  area (8 out of 9 original XMM pointings) in the North Galactic Pole region and we have detected 4 candidate X-ray clusters. We have then applied a new cluster finding algorithm on the SDSS galaxy distribution in this region, which is based on merging two independent selection methods - a smoothing-percolation SMP technique, and a Matched Filter Algorithm (MFA). Our final optical cluster catalogue, called the SMPMFA list, counts 9 candidate clusters with richness of more than 20 galaxies, corresponding roughly to the APM richness limit.

Out of the 4 X-ray candidate clusters 3 are common with our SMPMFA list. This relatively, small number of optical SMPMFA cluster candidates observed in X-rays suggest that some of the optical cluster candidates are either projection effects or poor X-ray emitters and hence they are fainter in X-rays than the limit of our shallow survey  $f_x(0.3-2\text{keV}) \simeq 2 \times 10^{-14} \text{erg cm}^{-2} \text{s}^{-1}$ . This latter explanation seems to be supported from an analysis of public XMM-Newton fields with larger exposure times.

## ACKNOWLEDGMENTS

We thank an anonymous referee for many useful comments that help improve this work. This research was jointly funded by the European Union and the Greek



Government in the framework of the project 'X-ray Astrophysics with ESA's mission XMM'. within the program 'Promotion of Excellence in Technological Development and Research'. MP also acknowledges funding by the Mexican Government grant No. CONACyT-2002-C01-39679.

## REFERENCES

- Abell, G.O., Corwin, H.G., Olowin, R.P., 1989, ApJS, 70, 1  
 Bahcall, N.A., 1988, ARA&A, 26, 631  
 Bahcall, N.A., & Lubin, L. M., 1993, ApJ, 415, L17  
 Bahcall, N.A., et al., 2003, ApJS, in press, astro-ph/0305202  
 Basilakos S., Plionis M., Maddox S. J., 2001, MNRAS, 316, 779  
 Bertin, E., & Arnouts, S., 1996, A&AS, 117, 393  
 Blanton M.R., et al., 2003, ApJ, 592, 819  
 Böhringer H., 1995, Large Scale Structure in the Universe, Proc. of an International Workshop, Potsdam Germany, 18-24 September 1994. Ed. by Jan P. Mücke, Stefan Gottloeber, and Volker Müller. Singapore: World Scientific, 1995, p.181  
 Böhringer H., et al. , 2001, A&A, 369, 826  
 Borgani, S., & Guzzo, L., 2001, Nature, 409, 39  
 Bruzual A.G., & Charlot, S. 1993, ApJ, 405, 538  
 Carlberg, R.G., Yee, H.K.C., Ellingson, E., Abraham, R., Gravel, P., Morris, S., Pritchet, C. J., 1996, ApJ, 369, 16  
 Carter, D. & Metcalfe, J., 1980, MNRAS, 191, 325  
 Castander, F.J., et al., 1995, Nature, 377, 39  
 Cavaliere, A., & Fusco-Femiano R., 1976, A&A, 49, 137  
 Couch, W.J., Ellis, R. S., MacLaren, I., Malin, D. F., 1991, MNRAS, 249, 606  
 Dalton, G.B., Efstathiou, G., Maddox, S. J., Sutherland, W. J., 1994, MNRAS, 269, 151  
 Donahue, M., et al., 2002, ApJ, 569, 689  
 Ebeling, H., et al., 1996a, Proc. Roentgenstrahlung from the Universe, MPE, Report 263, ed. H. U. Zimmerman, J. Trümper, H. Yorke (ISSN 0178-1719), 579  
 Ebeling, H., Voges, W., Böhringer H., Edge, A. C., Huchra, J. P., Briel, U. G., 1996B, MNRAS, 281, 799  
 Ebeling, H., et al., 2000, ApJ, 534, 133  
 Frenk, C. S., White, S. D. M., Efstathiou, G., Davis, M., 1990, ApJ, 351, 10  
 Fukugita, M., Shimasaku, K., Ichikawa, T. 1995, PASP, 107, 945  
 Georgakakis, A., et al., 2004, MNRAS, in press (*astro-ph/0305278*)  
 Gioia, I. M., Henry, J. P., Mullis, C. R., Voges, M., Briel, U. G., Böhringer H., Huchra, J. P., 2001, ApJ, 553, L105  
 Girardi, M., Biviano A., Giuricin G., Mardirossian F., Mezzetti M., 1995, ApJ, 438, 527  
 Girardi, M., Giuricin G., Mardirossian, F., Mezzetti M., Boschin W., 1998, ApJ, 505, 74  
 Gladders, M. D., & Yee, H. K. C., 2000, AJ, 120, 2148  
 Goto, T., et al., 2002, AJ, 123, 1807  
 Jones, C., Forman, W., 1999, ApJ, 511, 65  
 Lidman, C. E., & Peterson, B. A., 1996, AJ, 112, 2454  
 Lumsden, S. L., Nichol, R.C., Collins, C. A., Guzzo, L., 1992, MNRAS, 258, 1  
 Nichol, R. C., 2002, in ASP Conf. Ser., Tracing Cosmic Evolution with Galaxy Clusters, ed. S. Borgani, M. Mezzetti, R. Valdarnini, 268, 57  
 Olsen, L. F., et al., 1999, A&A, 345, 681  
 Postman, M., Lubin, L.M., Gunn, J. E., Oke, J.B., Hoessel, J.G., Schneider, D.P., Christensen, J.A., 1996, AJ, 111, 615  
 Pozzetti, L., Bruzual A., G., Zamorani, G., 1996, MNRAS, 281, 953  
 Rosati, P., Borgani, S., Norman, C., 2002, ARA&A, 40, 539  
 Scharf, C. A., Jones, L. R., Ebeling, H., Perlman, E., Malkan, M., Wegner, G., 1997, ApJ, 477, 79  
 Stocke, J. T., Morris, S. L., Gioia, I. M., Maccacaro, T., Schild, R., Wolter, A., Fleming, T. A., Henry, J. P., 1991, ApJS, 76, 813  
 Stoughton, C., et al., 2002, AJ, 123, 485  
 Sutherland, W., 1988, MNRAS, 234, 159  
 West, M. J., Jones, C., Forman, W., 1995, ApJ, 451, L5  
 York, D. G., et al., 2000, AJ, 120, 1579  
 Zwicky, F., Herzog, E., Wild, P., 1968, Pasadena: California Institute of Technology (CIT), 1961-1968